Bragg reflection from cholesteric liquid crystals

W. D. St. John, W. J. Fritz, Z. J. Lu, and D.-K. Yang
Liquid Crystal Institute, Kent State University, Ohio 44242
(Received 2 August 1994)

In this paper we discuss the optical reflective properties of single and multidomain cholesteric liquid crystals both experimentally and theoretically. The multidomain system has been prepared by dispersing a low concentration of polymer in a cholesteric liquid crystal. This results in a (passive) bistable colorful reflective display. Here we discuss the role of the polymer in altering the reflective properties in regard to their spectra and viewing characteristics. Theoretically we offer an application of the well known Berreman method [J. Opt. Soc. Am. **62**, 502 (1972)] suitable for systems composed of an ensemble of uncorrelated domains, each of which is composed of the same dielectric anisotropy, however with its own local orientation. Using this technique the reflective properties of a cholesteric liquid crystal possessing a distribution in the orientation of the helix axes are simulated. We furthermore illustrate how a small fluctuation in the pitch from one domain to another significantly reduces any interference fringes. From these simulations we will show how experimentally by using a polymer network one may control the extent to which the orientation of the helix axes are distributed.

PACS number(s): 61.30.−v

I. INTRODUCTION

Cholesteric liquid crystals are of great interest for display applications. When either a small amount of polymer is dispersed in the liquid crystal or when cells used have suitably treated surfaces, the system becomes bistable with no applied field. The two stable states are the planar and focal conic textures. When a cholesteric liquid crystal is in the planar texture the helix axes are perpendicular to the surface of the cell and the material reflects brilliant colored light determined by the pitch. When the liquid crystal is in the focal conic texture, the orientation of the helix axes are broadly distributed lending the material scattering. The ease of which these systems are made bistable coupled with the reflecting properties of their chiral nature, as well as the ability to control the pitch, make these systems well suited for passive reflective color displays [1–3].

In order to improve or optimize the reflective properties of these systems we (1) investigate the role of those material parameters which we may control and (2) model the effect of the polymer network (i.e., the multidomain system). As such we discuss the reflective properties of cholesteric liquid crystals with and without a polymer when in the planar state.

Because of their chiral and periodic structure cholesteric liquid crystals Bragg reflect circularly polarized light peaked at a wavelength given by the Bragg formula $\lambda_0=\bar{n}P_0$, where $\bar{n}$ is the average refractive index and P_0 is the pitch. The spectral width of the reflection peak is given by $\Delta\lambda=P_0\Delta n$, where Δn is the birefringence. Neglecting for the present discussion any refraction at the interface, when light is incident on a perfect planar texture obliquely at some angle θ_i the reflected light will only be detected at the angle $\theta_{\rm det}$ satisfying the Bragg condition which for the planar case is $\theta_{\rm det}=\theta_i$. The reflection will then be peaked at the wavelength $\lambda=\lambda_0\cos\theta_i$. For the nonplanar case, that is, the helix axis oriented at some angle θ with respect to the surface normal, our formulas are modified slightly and we have $\theta_{\rm det}=\theta_i-2\theta$ and $\lambda=\lambda_0\cos(\theta_i-\theta)$. In order to improve the viewing angle it is desired to make the helix axes have a distribution about the normal of the surface of the cell. This can be achieved either by dispersing some polymer throughout the liquid crystal or by using cells with rough surfaces. The polymer, in the course of being polymerized, will form a skeletal network which acts to create domains. The boundaries of these domains form a defect and are weakly scattering. The effect of these boundaries is to misorient the internal helices from planar. Similarly a rough surface will create defects and subsequently disturb the orientation of the helix axes. The planar texture with such a distribution is called the imperfect planar texture.

The results section of this paper is essentially twofold. Firstly, we discuss the reflective properties of the perfect planar texture, that is a single domain system. Here we show the effect of birefringence, cell thickness, angle of incidence, and polarization. Our motivation here derives from an application perspective, namely, how to optimize the reflective properties. Secondly, we discuss the imperfect planar texture, that is a multidomain system. This portion of the paper deals theoretically and experimentally with the polymer stabilized cholesteric texture (PSCT) display [4]. We illustrate that the imperfect planar texture may be suitably modeled as an ensemble of single layered, uncorrelated, Bragg reflecting domains. The net reflection is then calculated by weighting the independent reflections from each domain by some phenomenological distribution function.

In the foregoing we have used the Berreman method [5] to calculate the reflectivity. This method is very useful for cholesteric liquid crystals. However, this technique requires that the anisotropy only vary along a sin-

gle coordinate. Our application of this well known method is to our knowledge unique in that we apply this technique to systems which possess a distribution in the orientation of a given anisotropy, that is, the multidomain cholesteric liquid crystal. We do this by defining the fields external to the liquid crystal medium in a laboratory frame. The fields within the liquid crystal medium are then defined in a local frame whereby each domain possesses its own local coordinate system. We apply the Berreman method in the usual way to propagate the fields within the liquid crystal medium and then use a transformation matrix unique to a given domain to match the fields at the boundaries. Furthermore, the total reflectivity is a *weighted sum* over all domains. This allows us to define a distribution function for the orientation of the helix axes. Experimentally the extent of this distribution is controlled by the polymer concentration. Because the polymer network forms in space randomly and because the incident light used in these experiments is incoherent we add the reflected powers from each domain as opposed to the reflected fields. Hence we refer to this system as an ensemble of uncorrelated domains.

II. THEORY

The multidomain cholesteric medium in this study consist of a chiral-nematic liquid crystal combined with a low concentration of polymer. Our aim is to establish quantitatively the influence of the polymer as manifested in the reflective spectra. Our approach is to apply the Berreman method to calculate the reflectivity of a single domain whereby our definition of a single domain is that all helix axes lie parallel. The multidomain system is then treated as an ensemble of independent single domains whereby such properties as the pitch and helix orientation for each individual domain are independent of the properties of its neighbors. In this way we have treated the multidomain system as an incoherent random distribution of independently reflecting domains. The total power reflected for the ensemble then being a weighted average of the individual powers reflected. Our model only treats a single layered system, that is, any light ray only traverses a single domain. Furthermore, the problem is treated in two dimensions, thus all wave vectors lie in a single plane. The perfect planar system, that is, a system without any polymer, is simply a single-domain system. First we will show the formalism for a single domain (Sec. II A) and then the extension to a multidomain system (Sec. II B).

A. Reflectivity for a single domain

Here in a succinct manner we show the formalism of the Berreman method applied to the nonplanar cholesteric texture for a single domain. The distinction of this application from that of previously known applications of the Berreman method is that the nonplanar orientation of the cholesteric helix requires that a local coordinate system be established for each independent domain. Without this coordinate transformation the Berreman method could not be applied to the nonplanar multidomain system. The application of the Berreman method requires that the dielectric tensor only vary along one coordinate. We designate an unprimed coordinate system for the laboratory frame. In this frame the z axis is normal to the air-liquid crystal interface. All fields exterior to the liquid crystal medium are defined in this frame. In order to apply the Berreman method within the liquid crystal medium we must choose some local frame (the primed coordinate system) such that the dielectric tensor only varies along one coordinate. Thus a local frame is chosen such that the z' axis lies along the helical axis of the cholesteric medium. Within this local frame the dielectric tensor for a uniaxial chiral-nematic liquid crystal may be expressed as [6]

$$\vec{\vec{\varepsilon}}=\begin{bmatrix}\varepsilon_{11} & \varepsilon_{12} & 0\\ \varepsilon_{12} & \varepsilon_{22} & 0\\ 0 & 0 & \varepsilon_{33}\end{bmatrix}=\begin{bmatrix}\bar{\varepsilon}+\bar{\varepsilon}\delta\cos qz' & \beta\bar{\varepsilon}\delta\sin qz' & 0\\ \beta\bar{\varepsilon}\delta\sin qz' & \bar{\varepsilon}-\bar{\varepsilon}\delta\cos qz' & 0\\ 0 & 0 & \varepsilon_3\end{bmatrix}, \tag{1}$$

where in this notation, $\bar{\varepsilon}=(\varepsilon_1+\varepsilon_2)/2$, $\delta=(\varepsilon_1-\varepsilon_2)/(\varepsilon_1+\varepsilon_2)$, $q=(4\pi)/P$, $\beta=\pm 1$ (screw sense), and ε_3 (or $\varepsilon_\perp$)$=\varepsilon_2<\varepsilon_1$ (or $\varepsilon_\parallel$). Here the dielectric constants are real, that is, we have not included any absorptive effects [7]. We make the following definition:

$$\vec{\Psi}'=(E_x'E_y'H_x'H_y')^T . \tag{2}$$

From Maxwell's equations we then have

$$\frac{\partial\vec{\Psi}'}{\partial z'}ik_0\vec{\vec{Q}}(z')\cdot\vec{\Psi}' ,$$

where $\vec{\vec{Q}}(z')$ is a 4×4 matrix. For sufficiently small increments in z', $\Delta z'$, the approximate solution to $\vec{\Psi}'$ is

$$\vec{\Psi}'(z'+\Delta z')=e^{ik_0\vec{\vec{Q}}(z')\Delta z'}\cdot\vec{\Psi}'(z') . \tag{3}$$

For a cell of thickness d we have,

$$\vec{\Psi}'(d)=\prod_{p=1}^{p_{\max}=d/\Delta z'} e^{ik_0Q(d-p\Delta z')}\cdot\vec{\Psi}'(0)=\vec{\vec{F}}\cdot\vec{\Psi}'(0) \tag{4}$$

or

$$\vec{\Psi}'(0)=\vec{\vec{F}}^{-1}\cdot\vec{\Psi}'(d) . \tag{5}$$

We note that we have used the *faster* Berreman method [8]. This distinction refers to how the exponential in Eq. (3) is treated. By invoking the Cayley-Hamilton theory [9] as opposed to a straightforward Taylor series expansion one arrives at an exact truncated series as opposed to an approximate truncated series for the exponential. The former technique allows much larger values of $\Delta z'$ to be used with comparable accuracy, hence it has been named the *faster* Berreman method. We now make the transformation from the local (primed) frame to the laboratory (unprimed) frame by the following transformation:

$$\vec{\Psi}=\vec{\vec{A}}\cdot\vec{\Psi}' , \tag{6}$$

where

$$\overleftrightarrow{A}=\begin{bmatrix}\cos\theta & 0 & 0 & \bar{n}\eta_0\sin(\theta-\theta_r)\sin\theta/\varepsilon_3 \\ 0 & 1 & 0 & 0 \\ 0 & -\bar{n}\eta_0\sin(\theta-\theta_r)\sin\theta/\varepsilon_3 & \cos\theta & 0 \\ 0 & 0 & 0 & 1\end{bmatrix}, \tag{7}$$

$\bar{n}$ is the average refractive index of the dielectric medium, η_0 is the impedance in a vacuum, and θ_r is the refracted angle at the top surface ($z=0$). Equation (7) is not simply a transformation between the two coordinate systems but rather a transformation for the fields expressed in the two coordinate systems. Using Eqs. (5) and (6), and the usual boundary conditions we have

$$\vec{\Psi}^i=-\vec{\Psi}^r+\overleftrightarrow{A}\cdot\overleftrightarrow{F}^{-1}\cdot\overleftrightarrow{A}^{-1}\cdot\vec{\Psi}^t=-\vec{\Psi}^r+\overleftrightarrow{H}\cdot\vec{\Psi}^t\ , \tag{8}$$

where r, i, and t indicate reflected, incident, and transmitted, respectively. Because the medium external to the liquid crystal is uniform (isotropic) the magnetic field components may be simply expressed in terms of their respective electric field components. Finally, upon expressing all fields in terms of the usual $\hat{\pi}$ and $\hat{\sigma}$ polarizations, we arrive at the solution for both the reflected and transmitted fields in terms of the known incident fields,

$$\begin{bmatrix}E^r_\pi \\ E^r_\sigma \\ E^t_\pi \\ E^t_\sigma\end{bmatrix}=\overleftrightarrow{M}\cdot\begin{bmatrix}E^i_\pi \\ E^i_\sigma \\ E^i_\sigma \\ E^i_\pi\end{bmatrix}. \tag{9}$$

Lastly we note that we have matched the ambient refractive index with the average refractive index of the liquid crystals so as to cancel any Fabry-Pérot fringes, however by use of Snell's law we have still used the true angles of refraction [10]. With this technique we are able to include refraction without reflection at the air-liquid crystal interface.

B. Extension to a multidomain system

Let $R_{mn}(\theta_m,P_n)$ represent the power reflected from domain (mn). The individual domains are parametrized by the orientation of the helix (now subscripted) θ_m and the pitch P_n. The total reflected power for the ensemble is then given by

$$R_T=\int_{\theta_m}\int_{P_n}R_{mn}f(\theta_m)g(P_n)d\theta_m dP_n\ , \tag{10}$$

where $f(\theta_m)$ and $g(P_n)$ are resolved phenomenologically. The distribution functions arise from the deviation from a perfect planar structure. Experimentally the deviation from a perfect planar texture is controlled by the polymer concentration. For the case of the helix orientation we found it necessary to use two Gaussian functions for the highest polymer concentration. Here the experimental results clearly show two distinct regions thus requiring a relatively narrow Gaussian together with a much broader Gaussian. For the lower polymer concentrations a single Gaussian sufficed. We have used the following distribution functions,

$$f(\theta_m)=A_1\frac{\exp(-\theta_m^2/2\sigma_1^2)}{\sigma_1}+A_2\frac{\exp(-\theta_m^2/2\sigma_2^2)}{\sigma_2}$$
$$\text{where}\ \int_{-\pi/2}^{\pi/2}f(\theta_m)d\theta_m=1 \tag{11}$$

and

$$g(P_n)=\frac{\exp[-(P_n-P_0)^2/2\sigma_p^2]}{\sqrt{2\pi\sigma_P^2}}$$
$$\text{where}\ \int_0^\infty g(P_n)dP_n=1\ . \tag{12}$$

In the latter P_0 is the unperturbed pitch fixed at 0.54 μm. We stress that the assignment of these distribution functions was entirely phenomenological.

III. EXPERIMENT

The incident light source is composed of a voltage regulated tungsten-halogen lamp and the reflectivity is detected by a SpectraScan ^{PR}704 spectrum analyzer equipped with a telescopic lens. Polarization states are achieved with broadband sheet polarizers. For all cases the cholesteric liquid crystal is a chiral-nematic mixture comprised of 72 wt % E48 (nematic) and 28 wt % chiral. The chiral component is a mixture of CE1, CB18, and R1011. (All liquid crystal materials by E. Merck.) This particular composition of chiral and nematic components strongly reflects "green" light with a pitch $\sim$0.34 μm (or

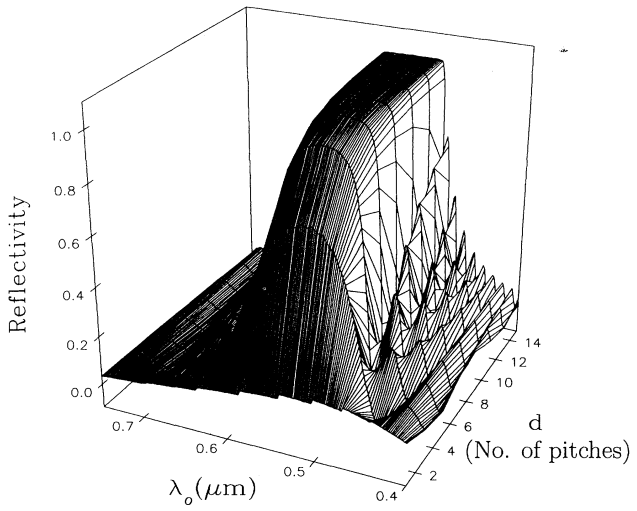

FIG. 1. Reflection spectra versus cell thickness. $P_0=0.54$ μm and $\Delta n=0.228$.

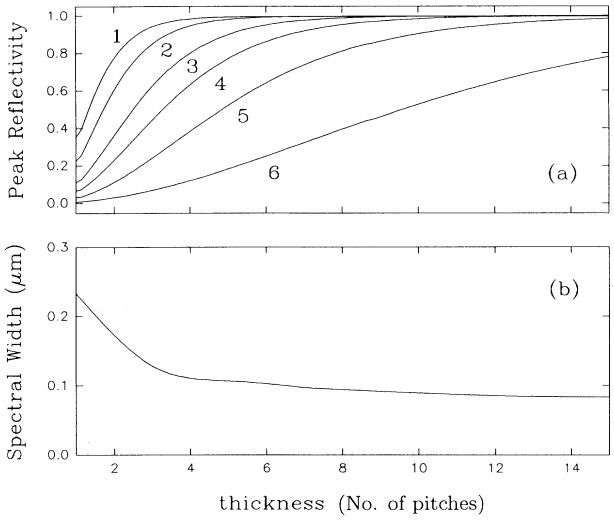

FIG. 2. Peak reflectivity (top) and spectral width at FWHM (bottom) versus the cell thickness. The peak reflectivity is parametrized by the birefringence with (1) $\Delta n=0.35$, (2) $\Delta n=0.3$, (3) $\Delta n=0.25$, (4) $\Delta n=0.20$, (5) $\Delta n=0.15$, and (6) $\Delta n=0.10$. Below the birefringence is fixed at $\Delta n=0.228$.

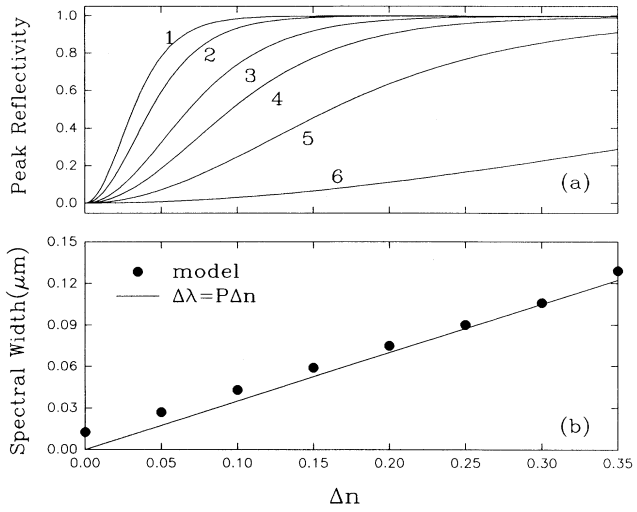

FIG. 4. Peak reflectivity (top) and spectral width at FWHM (bottom) versus the birefringence. The peak reflectivity is parametrized by the cell thickness (d) in units of the pitch (P_0) and (1) $d=15P_0$, (2) $d=11P_0$, (3) $d=7P_0$, (4) $d=5P_0$, (5) $d=3P_0$, and (6) $d=P_0$.

a vacuum wavelength of ~ 0.54 μm). The cell is surface treated with polyimide and indium tin oxide and the mixture vacuum filled. For those cells containing polymer the liquid crystal is homeotropicaly aligned with an applied field during photopolymerization.

IV. RESULTS AND DISCUSSION

A. Perfect planar texture

Firstly we consider the effect of cell thickness on the reflectivity of a perfect planar texture. In Fig. 1 we show

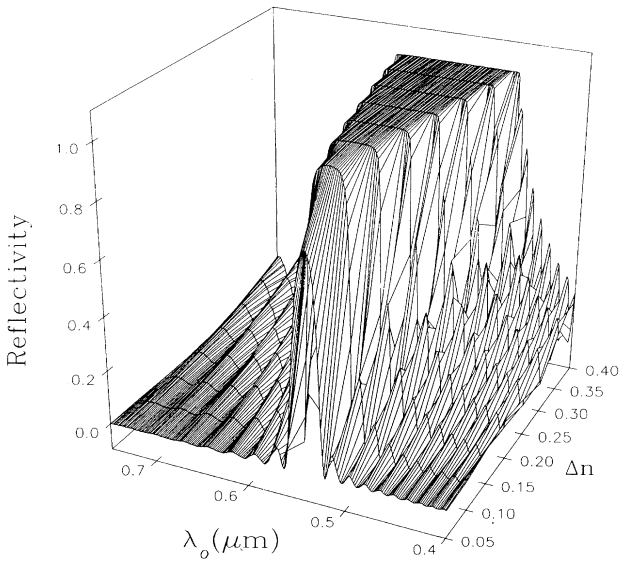

FIG. 3. Reflection spectra versus the birefringence. $P_0=0.54$ μm and $d=15P_0$.

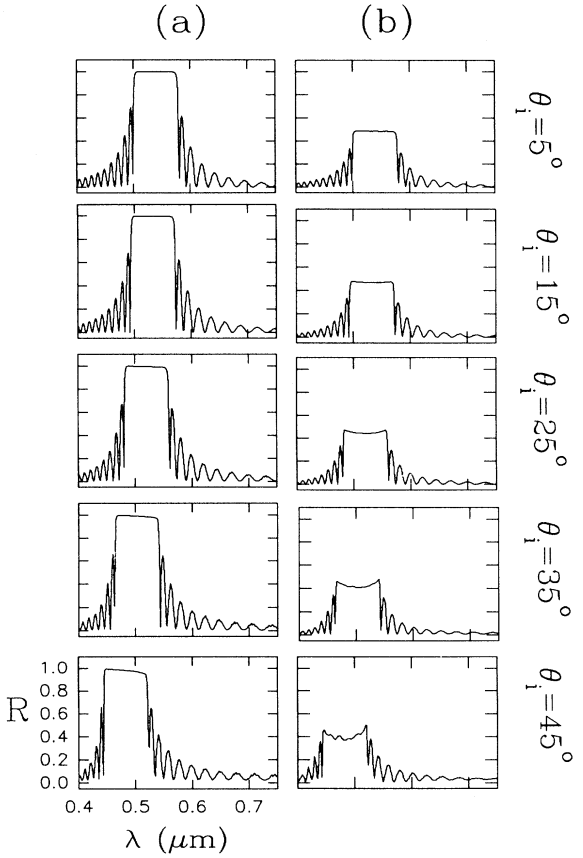

FIG. 5. Theoretical reflection spectra for (a) incident right circular polarization and (b) unpolarized light at five angles of incidence, θ_i.

a theoretical simulation of the reflection spectra as a function of the cell thickness. We have selected the following parameters: $\Delta n = 0.228$, $\bar{n} = 1.63$, and $\bar{n}P_0 = 0.54$ μm. The light is incident normally and right circular polarized. The sense of the liquid crystal helices is the same. All the reflected light is collected. Due to the circular nature of the cholesteric medium incident circularly polarized light with a rotational sense equal to that of the liquid crystal helices will be strongly reflected. The counter circular polarization state will be strongly transmitted. As Fig. 1 illustrates, for a sufficient number of layers such incident light is completely reflected and although not apparent from this figure, completely right circular polarized. In Figs. 2(a) and 2(b) we show the maximum reflectivity as a function of the cell thickness with the birefringence as a parameter (top) and the spectral width [full width at half maximum (FWHM)] as a function of the cell thickness at a single birefringence (bottom). If it were desired to minimize the cell thickness, in order to optimize the switching dynamics, for example, this simulation illustrates that a cell thickness of ~ 6 pitch lengths is sufficient. In Fig. 3 we similarly illustrate the results of a varying birefringence for a cell thickness of $15P_0$. In Fig. 4(a) (top) we show the peak reflectivity as a function of the birefringence with the cell thickness parametrized and in Fig. 4(b) (bottom) the spectral width (FWHM) as a function of the birefringence with a cell thickness of $15P_0$. From Fig. 4(a) we see that the reflection is maximized beyond a birefringence of ~ 0.1 and that the spectral width linearly increases with the birefringence, as is well known.

Next we consider the reflection spectra for obliquely incident light and varying polarizations. In Fig. 5 we have light incident with (a) right circular polarization and (b) unpolarized light. We show the results at five angles of incidence. Note at near normal incidence the peak reflection is $\sim 100\%$ for the case of right circular polarization and $\sim 50\%$ for an unpolarized source (only the right circular component is reflected). In both cases we see the expected spectral shift towards shorter wavelengths as the angle of incidence is increased. Additionally we see in both cases an increase in structure present in the center fringe.

In Fig. 6 we show the case of linear polarized light. In this scenario we have $\hat{\sigma}$-polarization incident and $\hat{\pi}$-polarization reflected ($R^{\sigma\pi}$). This choice of polarizations corresponds to the use of crossed polarizers. Here we also show the experimental results. Our theoretical simulations are shown in columns (a) and (b) while the experimental results are shown in column (c). The two theoretical simulations illustrate the effect of a fluctuating pitch. In column (a) we have a fixed pitch ($P_0 = 0.54$ μm) and in column (b) we have allowed the pitch to fluctuate according to $g(P_n)$ previously defined by Eq. (12) with

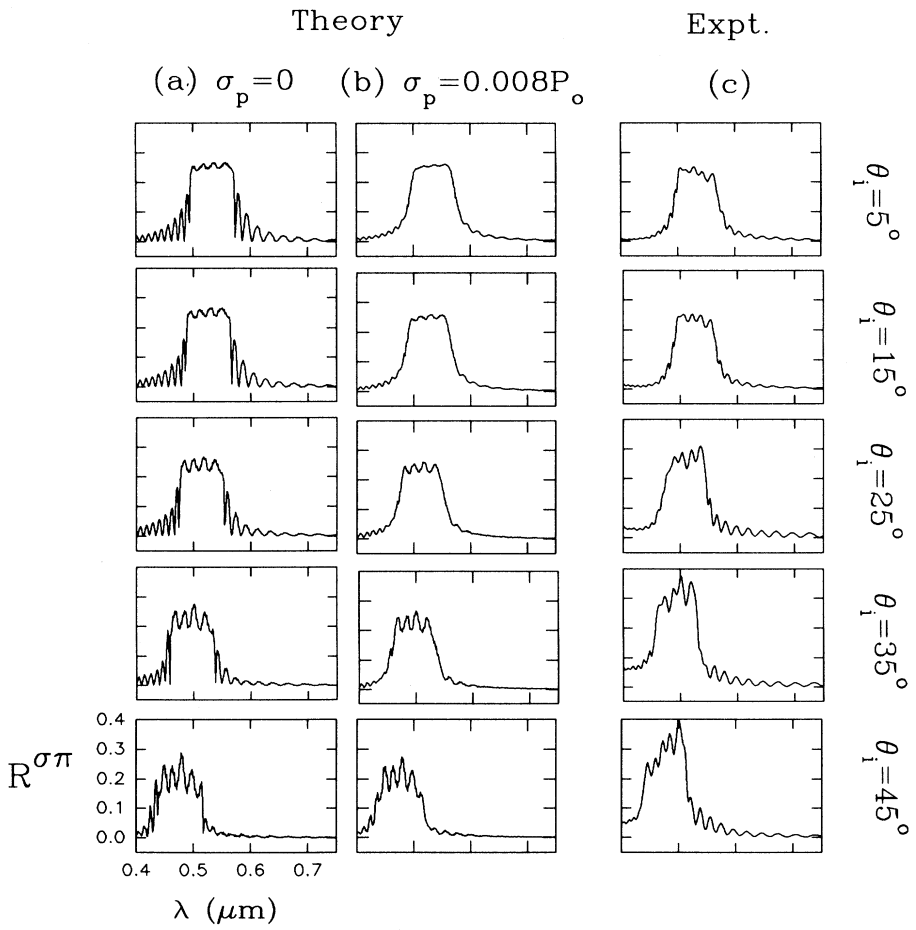

FIG. 6. Theoretical (a and b) and experimental (c) reflection spectra for the case of crossed polarizers, i.e., incident $\hat{\sigma}$ polarization and reflected $\hat{\pi}$ polarization. In Fig. (a) the pitch is fixed while in Fig. (b) the pitch fluctuates by $\sim 1\%$ ($\sigma_p = 0.008P_0$).

$\sigma_P = 0.008 P_0$ (i.e., $\sim 1\%$ fluctuation). Obviously the case of a fluctuating pitch more closely resembles that of the experiment.

From an application point of view one would like the cell, or display, to be as thin as possible. This makes the system more compact in addition to decreasing the necessary drive voltage and increasing the switching speed. However, one must be careful not to make the cell so thin as to reduce the reflectivity significantly. According to the theoretical simulation a 3 μm and 5 μm cell should have the same reflectivity. We prepared two cells with the aforementioned cell gaps. This corresponds to cell gaps slightly less than 9 and 15 pitch lengths. According to the theory we should expect approximately equal peak reflectivities. For these pure cholesteric liquid crystals the perfect planar texture is expected. The reflection spectra using crossed polarizers (i.e., $R^{\sigma\pi}$) for the two cells are approximately the same as is shown in Fig. 7 thus supporting the theoretical simulation. The relative spectral shift is due to the quantization of the pitch induced by the boundary conditions.

B. Imperfect planar texture

Next we consider how the introduction of a polymer network effects the reflective spectra. Here we have prepared three cells with varying amounts of polymer. Our intuition is that the polymer will force the orientation of the helix axes away from that of a perfect planar texture resulting in the imperfect planar texture. Preparing the cells in this way creates a multidomain system bistable in the focal conic and imperfect planar textures. The liquid crystal is again the same as described above.

In Fig. 8 we show the experimental spectra obtained for the three polymer concentrations. Here the angle of the incident light is 27° and we measure the reflection at the angles of $27° + \beta$ where $\beta = \{0°, 4°, 10°, 25°, \text{and } 40°\}$. This corresponds to helix orientations of $\theta = \{0°, 1.1°, 2.8°, 6.4°, \text{and } 9.1°\}$, respectively. (Refraction at the air-liquid crystal interface has been incorporated.) If in fact the polymer forces the helix axes to have some distribution in their orientation then we should expect an

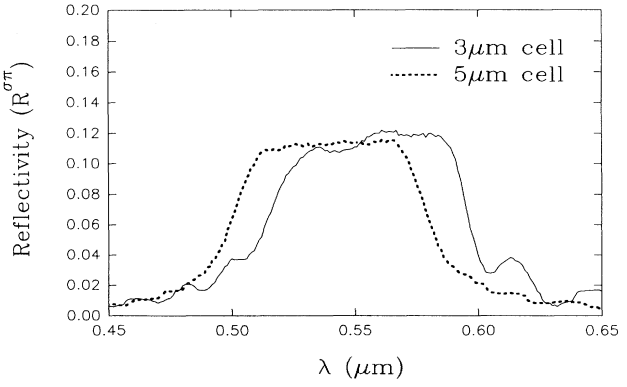

FIG. 7. Experimental reflection spectra at normal incidence for cell gaps of 3 and 5 μm.

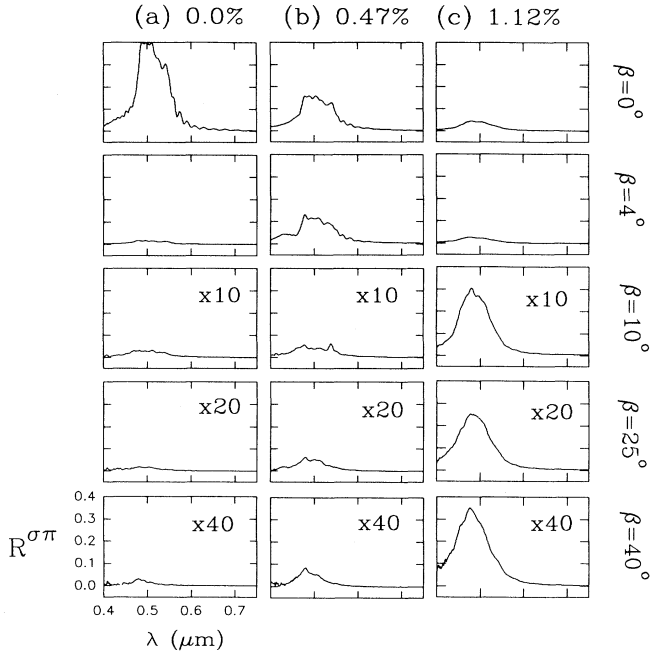

FIG. 8. Experimental reflection spectra for three polymer concentrations at and beyond the specular angle. The incident angle is 27° and the detection angle is $27° + \beta$.

enhancement in the reflectivity away from the specular angle with increasing polymer concentrations. As can be seen this is in fact true. We see for the case of (a) no polymer that the texture is very nearly that of a perfect planar texture as shown by the negligible reflection off the specular angle. In columns (b) and (c) we have a polymer concentration of 0.47% and 1.12%, respectively. We see that the polymer does in fact misorient the liquid crystal away from the perfect planar texture resulting in Bragg reflection off of the specular angle. Because the orientation of the helix axes is now distributed there exist a reduction in the reflection when at the specular angle simply because of a reduction in the number of domains which have the appropriate alignment of the helix axes to Bragg reflect at that angle. From an application standpoint the polymer effectively enhances the viewing angle. An unfortunate consequence of the polymer is that the defect volume increases resulting in a reduction in the brightness at all angles of view. We note that for the polymer concentrations of 0.47% and 1.12%, optical microscopy studies reveal an approximate domain size of ~ 50 μm down to a few micrometers, respectively.

Our theoretical goal here is essentially twofold. Firstly, we hope to verify our intuition in regard to envisaging the polymer as causing a distribution about the normal in the helix axes orientation and secondly, we hope to identify this distribution at least phenomenologically. In order to find this distribution we have compared the simulation with the experimental results of luminance versus detection angle. Here the luminance is simply the integrated spectra. The results of experiment and theory are shown in Fig. 9. Our fitting parameters here are for

that of $f(\theta_m)$, namely, A_1, A_2, σ_1, and σ_2 [see Eq. (11)]. We again stress that our choice for $f(\theta_m)$ is entirely based on phenomenology and that we offer no physical argument from first principles. For the cases of (a) 0.0% and (b) 0.47% polymer concentration only a single Gaussian was necessary, however for the case of (c) 1.12% polymer concentration two Gaussian functions were necessary. As can be seen for the latter case there seems to exist two regions in the luminance characterized by a relatively sharp reduction in the reflectivity for small deviations away from the specular angle and a relatively broad region for larger detection angles hence the necessity for the second Gaussian. Thus for the higher concentration of polymer the helix axes become oriented at relatively large angles with respect to the normal. Using this as our means to identify the distribution function we now compare the reflection spectra weighted by this distribution function with the experimental reflection spectra. In Fig. 10 we show the theoretical reflection spectra for a multidomain texture with a fixed pitch ($P_0=0.54$ μm) and in Fig. 11 similar calculations, however with the addition of a fluctuating pitch. In the latter the pitch is distributed again by $g(P_n)$ previously defined by Eq. (12) with $\sigma_p=0.06P_0$ (i.e., $\sim 6\%$ fluctuation). Comparing these simulations with the experimental results in Fig. 8 we see that the agreement is quite good with the inclusion of a fluctuating pitch. For these calculations it is apparent that the deviation from the perfect planar texture imposed by the polymer network is re-

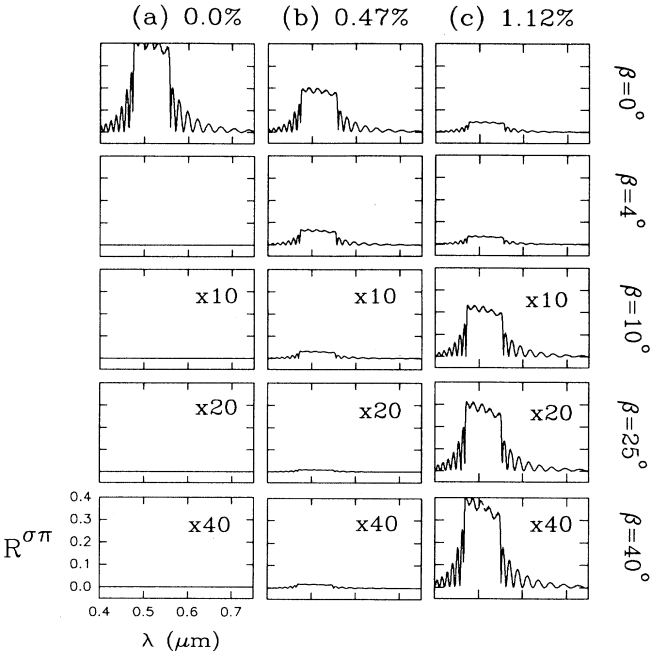

FIG. 10. Theoretical reflection spectra for the three polymer concentrations at and beyond the specular angle. The incident angle is 27° and the detection angle is 27°+β. The pitch is held fixed at 0.54 μm (i.e., $\sigma_P=0.0$).

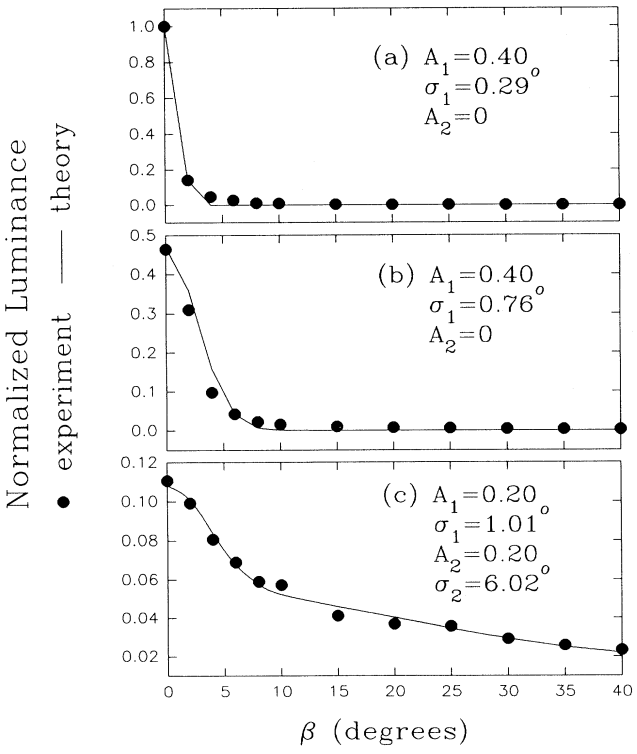

FIG. 9. Experimental and theoretical luminance (integrated spectra) versus the detection angle for all three polymer concentrations of (a) 0.00%, (b) 0.47%, and (c) 1.12%.

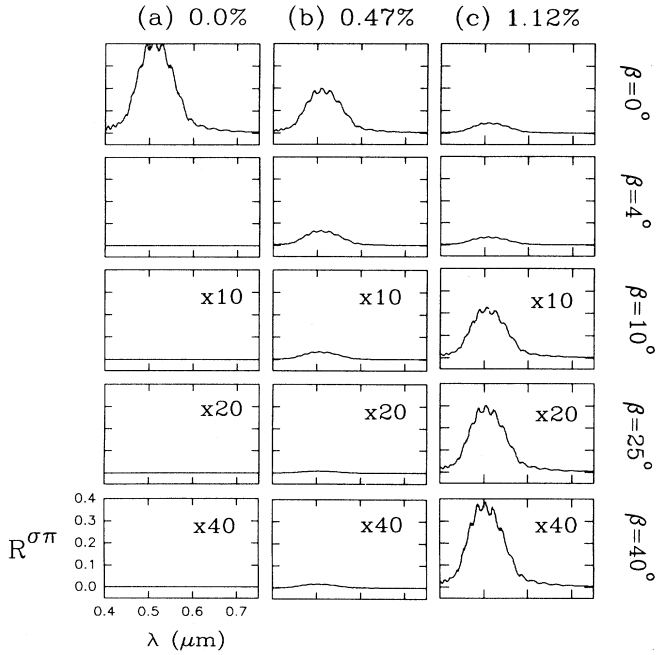

FIG. 11. Theoretical reflection spectra for the three polymer concentrations at and beyond the specular angle. The incident angle is 27° and the detection angle is 27°+β. The pitch fluctuates by $\sim 6\%$ (i.e., $\sigma_p=0.06P_0$).

sponsible for the enhanced reflection away from the specular angle and that a relatively small fluctuation in the pitch is sufficient to explain the negligible interference fringes.

V. CONCLUSION

We have performed a number of simulations for the perfect planar texture in hopes of understanding the effects of birefringence, cell thickness, and polarization on the reflective spectra. This not only serves the purpose of exercising the model but also provides information on how to choose materials for optimizing the construction of reflective displays. We have further shown that a dispersed polymer in a cholesteric liquid crystal has the effect of distributing the orientation of the helix axes about the normal which acts to broaden the viewing angle as well as further smear any interference fringes. This effect has been verified from both the reflection spectra as well as the luminance when measured as a function of polymer concentration and detection angle. Our investigation shows that these materials are suitable for bistable (passive) colorful reflective display applications.

We have successfully modeled this system by assuming a single-layered multidomain system essentially composed of an ensemble of uncorrelated Bragg reflectors. The distribution in the helix orientation for the individual domains follows that of a Gaussian distribution. We have also assigned phenomenologically a Gaussian distribution for the pitch about some unperturbed value. It has been shown that a distribution on the order of 1% is sufficient in the case of no polymer and a pitch distribution on the order of 6% in the case of the highest polymer concentration. This was necessary in order to simulate the "washing out" of the interference fringes as seen experimentally.

ACKNOWLEDGMENTS

The authors express their appreciation for the many helpful discussions with Dr. R. M. Hornreich now at the Weizmann Institute of Science in Rehovot, Israel. This research was supported in part by the NSF Science and Technology Center ALCOM under Grant No. DMR89-20147.

[1] G. Dir *et al.*, Proc. SID **13**, 2 (1972).
[2] W. Greubel, U. Wolff, and H. Kruger, Mol. Cryst. Liq. Cryst. **24**, XX (1973).
[3] D.-K. Yang and J. W. Doane, Appl. Phys. Lett. **64**, 1905 (1994).
[4] J. W. Doane, D.-K. Yang, and Z. Yariv (unpublished).
[5] Dwight W. Berreman, J. Opt. Soc. Am. **62**, 502 (1972).
[6] S. Chandrasekhar, *Liquid Crystals,* 2nd ed. (Cambridge University Press, New York, 1992).
[7] J. Nehring, J. Chem. Phys. **75**, 4326 (1981).
[8] H. Whöler, G. Haas, M. Fritsch, and D. A. Mlynski, J. Opt. Soc. Am. A **5**, 1554 (1988).
[9] William L. Brogan, *Modern Control Theory,* 2nd ed. (Prentice-Hall, Englewood Cliffs, NJ, 1985).
[10] K. H. Yang, J. Appl. Phys. **68**, 1550 (1990).